

Coreless vortex formation in a spinor Bose-Einstein condensate

A.E. Leanhardt, Y. Shin, D. Kielpinski, D.E. Pritchard, and W. Ketterle*

Department of Physics, MIT-Harvard Center for Ultracold Atoms, and Research Laboratory of Electronics, Massachusetts Institute of Technology, Cambridge, Massachusetts, 02139

(Dated: October 24, 2018)

Coreless vortices were phase-imprinted in a spinor Bose-Einstein condensate. The three-component order parameter of $F = 1$ sodium condensates held in a Ioffe-Pritchard magnetic trap was manipulated by adiabatically reducing the magnetic bias field along the trap axis to zero. This distributed the condensate population across its three spin states and created a spin texture. Each spin state acquired a different phase winding which caused the spin components to separate radially.

PACS numbers: 03.75.Nt, 67.57.Fg, 03.65.Vf, 67.40.Db

Spin textures play a central role in describing the physics of elementary particles [1], liquid $^3\text{He-A}$ [2, 3, 4], the quantum Hall effect [5], and gaseous Bose-Einstein condensates [6, 7, 8, 9, 10]. Topological defects vary between superfluid systems described by scalar and vector order parameters. In spin-less or spin-polarized condensates, line defects such as vortices have cores where the density of condensed particles is necessarily zero to keep the order parameter single-valued [11, 12, 13]. However, in condensates with an internal, spin degree-of-freedom, coreless vortices exist as spin textures [4, 14]. Such structures are referred to as skyrmions (Anderson-Toulouse vortices [3]) or merons (half-skyrmions, Mermin-Ho vortices [2]) depending on the boundary conditions of the system.

In this Letter, we study spin textures in a Bose-Einstein condensate (BEC). Coreless vortices were created in $F = 1$ spinor condensates held in a Ioffe-Pritchard magnetic trap by adiabatically reducing the magnetic bias field along the trap axis to zero. This continuously transformed the initially spin-polarized condensate into a coherent superposition of three spin states, each with a different phase winding. The resulting angular momentum per particle varied between spin states and the condensate evolved such that states with more angular momentum per particle circulated around states with less angular momentum per particle. Thus, the condensate had a net axial magnetization that varied with radial position. Previous work on vortices in a two-component system used laser, microwave, and radio frequency fields to spatially and temporally control the interconversion between components [14]. However, without these applied fields the two-components evolved independently as distinguishable fluids. In our work, the spin states can freely interconvert at all points in space and time such that the spin texture would continually heal itself even in the presence of state-dependent losses.

In cylindrical coordinates, the spin- F condensate wavefunction can be written as $|\Psi(r, \phi, z)\rangle = \sqrt{n(r, \phi, z)}|\zeta(r, \phi, z)\rangle$, where n is the atomic number density and the $2F + 1$ component spinor $|\zeta\rangle = \sum_{m_z=-F}^F \zeta_{m_z}|F, m_z\rangle$, $|\langle\zeta|\zeta\rangle|^2 = 1$ describes a spin tex-

ture. A Ioffe-Pritchard magnetic trap consists of an axial bias field (with curvature) and a two-dimensional quadrupole field in the orthogonal plane [15, 16]:

$$\vec{B}(r, \phi, z) = B_z \hat{z} + B'r(\cos(2\phi) \hat{r} - \sin(2\phi) \hat{\phi}), \quad (1)$$

where B' is the radial magnetic field gradient and quadratic terms have been neglected. For a condensate of radial extent R confined in a Ioffe-Pritchard magnetic trap with $B_z \gg B'R > 0$, $|\zeta\rangle = |F, m_z = m_F\rangle$, where m_z and m_F are the projection of the atomic spin along the z -axis and local magnetic field direction, respectively. Adiabatically ramping B_z from $B_z \gg B'R > 0$ to zero rotates the atomic spin about the position-dependent axis $\hat{n}(\phi) = \sin\phi \hat{x} + \cos\phi \hat{y}$, and drives the transition $|F, m_z = m_F\rangle \rightarrow \sum_{m_z=-|m_F|}^{|m_F|} \zeta_{m_z} \exp(i(m_z - m_F)\phi) |F, m_z\rangle$ [17, 18]. Thus, the condensate population is distributed across $2|m_F| + 1$ spin states with each acquiring a different topological phase factor and angular momentum per particle due to the variation of Berry's phase with magnetic quantum number [19].

The condensate remains in the state $|F, m_F\rangle$ with respect to the local magnetic field provided the local Zeeman energy, $\sim g_F \mu_B (B_z^2 + (B'r)^2)^{1/2}$, dominates the local kinetic energy associated with the spin texture, $\sim \hbar^2/mr^2$, where g_F is the Landé g -factor, μ_B is the Bohr magneton, and m is the atomic mass. For $B_z = 0$, atomic spins aligned with the quadrupole magnetic field produce the planar spin texture in Fig. 1(a). However, the infinite kinetic energy associated with the wavefunction singularity at $r = 0$ creates a non-planar spin texture over a disc of radius $\sim (\hbar^2/mg_F\mu_B B')^{1/3}$, with higher angular momentum spin states residing outside those with lower angular momentum.

Bose-Einstein condensates containing over 10^7 ^{23}Na atoms were created in the $|1, -1\rangle$ state in a magnetic trap, captured in the focus of an optical tweezers laser beam, and transferred into an auxiliary "science" chamber as described in Ref. [21]. In the science chamber, the condensate was loaded into a microfabricated Ioffe-Pritchard magnetic trap formed by a Z-shaped $50 \mu\text{m} \times 10 \mu\text{m}$ electroplated copper wire carrying cur-

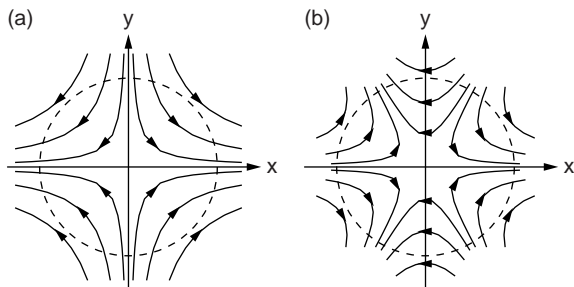


FIG. 1: Planar spin textures. Spins aligned with two-dimensional (a) quadrupole and (b) hexapole magnetic fields produce textures with winding numbers -1 and -2 , respectively. In general, spins aligned with a two-dimensional axisymmetric multipole magnetic field, $\vec{B} = Ar^{q-1}(\cos(q\phi)\hat{r} - \sin(q\phi)\hat{\phi})$, $q > 0$, produce a texture with winding number $-(q-1)$. Counter-clockwise traversal of the dashed contours in (a) and (b) leads to clockwise (negative) spin rotation, with the winding number defined as the integer number of revolutions made by the spin vector while circumnavigating the singularity at the origin [20].

rent I and an external magnetic bias field, B_{\perp} , as described in Ref. [22]. Typical wiretrap parameters were $I = 720$ mA, $B_{\perp} = 5.3$ G, and $B_z = 1.3$ G, resulting in a radial magnetic field gradient $B' = 180$ G/cm. This produced axial and radial trap frequencies $\omega_z = 2\pi \times 4$ Hz and $\omega_{\perp} = 2\pi \times 250$ Hz, respectively. Condensates in the wiretrap had $\geq 2 \times 10^6$ atoms, a Thomas-Fermi radius of ≈ 5 μm , and a lifetime ≥ 25 s [23].

Coreless vortices imprinted onto the condensate wavefunction by adiabatically ramping $B_z \rightarrow 0$ are shown in Fig. 2. To observe the nature of the spin texture, an axial bias field was switched on non-adiabatically along either the negative [Fig. 2(a)-(d)] or positive [Fig. 2(e)-(h)] z -axis. Switching the axial bias field on suddenly “froze” the atomic spins and effectively “projected” the condensate wavefunction onto a basis quantized with respect to the local (axial) magnetic field. This allowed the spin states to be separated by a magnetic field gradient applied during ballistic expansion. Switching the direction of the axial projection field exchanged the roles of the $|1, -1\rangle$ and $|1, +1\rangle$ states. Figures 2(a) and 2(e) show the coreless nature of the vortices, while Figs. 2(b) and 2(f) show the concentric cylinder structure resulting from the competition between the atomic Zeeman energy and the kinetic energy of the rotating spin states. We assume that the two-dimensional ($\omega_z \ll \omega_{\perp}$) ballistic expansion process simply magnifies the condensate wavefunction, as it does in the expansion of a single-component condensate with vortices [24, 25].

To imprint the coreless vortices, the axial bias field was ramped linearly from $B_z = 1.3$ G to $B_z \approx 0$ in 10 ms.

Along the wiretrap axis, the magnetic field was

$$\vec{B}(r=0, \phi, z) = (B_z + \frac{1}{2}B''z^2)\hat{z}, \quad (2)$$

where quadratic terms neglected in Eq. (1) are included. The presence of axial magnetic field curvature, $B'' \approx 5$ G/cm², implies that the spin texture had a slight axial dependence. Ramping $B_z \rightarrow 0$ quickly (10 ms) compared to the axial trap period (250 ms) compressed the condensate radially but left the axial extent of the condensate unchanged. Thus, the axial magnetic field variation, ΔB_z , was less than the radial magnetic field variation, ΔB_r , and the axial dependence of the spin texture was minimal. With $B_z = 1.3$ G ($B_z \approx 0$ G), the condensate chemical potential was $\mu \approx (\mu_B/2) \times 3$ mG ($\mu \approx (\mu_B/2) \times 27$ mG) yielding $\Delta B_z \approx 3$ mG ($\Delta B_r \approx 27$ mG). The images shown in Fig. 2 integrated the atomic number density along the z -axis and therefore averaged over the minor axial variation to the spin texture.

To project the condensate wavefunction onto a basis quantized with respect to the local magnetic field, an axial bias field was switched on at a rate of $\dot{B}_z = 2 \times 10^5$ G/s along either the negative or positive z -axis. For $0 \leq B_r \leq \Delta B_r$, the Landau-Zener non-adiabatic transition probability, $\exp(-\pi\mu_B B_r^2 / \hbar \dot{B}_z) \geq 0.9$, was sufficiently close to unity that the atomic spins remained “frozen” during the sudden application of the axial bias field and the spin texture could be accurately diagnosed. The magnetic trap was switched off 100 μs after applying the axial bias field allowing the atoms to expand ballistically. While the total condensate density monotonically decreased as a function of radial position [Figs. 2(a) and 2(e)], the density of each spin component peaked at a different radius signifying a variation in the angular momentum per particle between spin states [Figs. 2(b) and 2(f)].

With the application of a projection field along the positive z -axis, additional rings of atoms appeared in the $|1, -1\rangle$ and $|1, 0\rangle$ states [Fig. 2(f)]. Possible technical origins include the non-instantaneous turn on of the projection field and the ballistic expansion process. Also, ramping $B_z \rightarrow 0$ in 10 ms was non-adiabatic for atoms near $r = 0$ causing an atom loss of $\approx 50\%$ as observed in previous work [18]. If these atoms had not left the condensate before the projection field was applied, they may have contributed to the images displayed in Fig. 2(f). The additional rings of atoms may also correspond to a low energy, radial spin-wave excitation [6, 7]. However, we could not identify any asymmetry between applying the projection field along the positive versus negative z -axis that would account for the presence of the extra rings in Fig. 2(f) but not in Fig. 2(b).

Engineering topological states in a Bose-Einstein condensate has received much theoretical attention [17, 26, 27, 28, 29, 30]. The evolution of a condensate confined in a Ioffe-Pritchard magnetic trap while ramping $B_z \rightarrow 0$ is described by a position-dependent spin rotation about

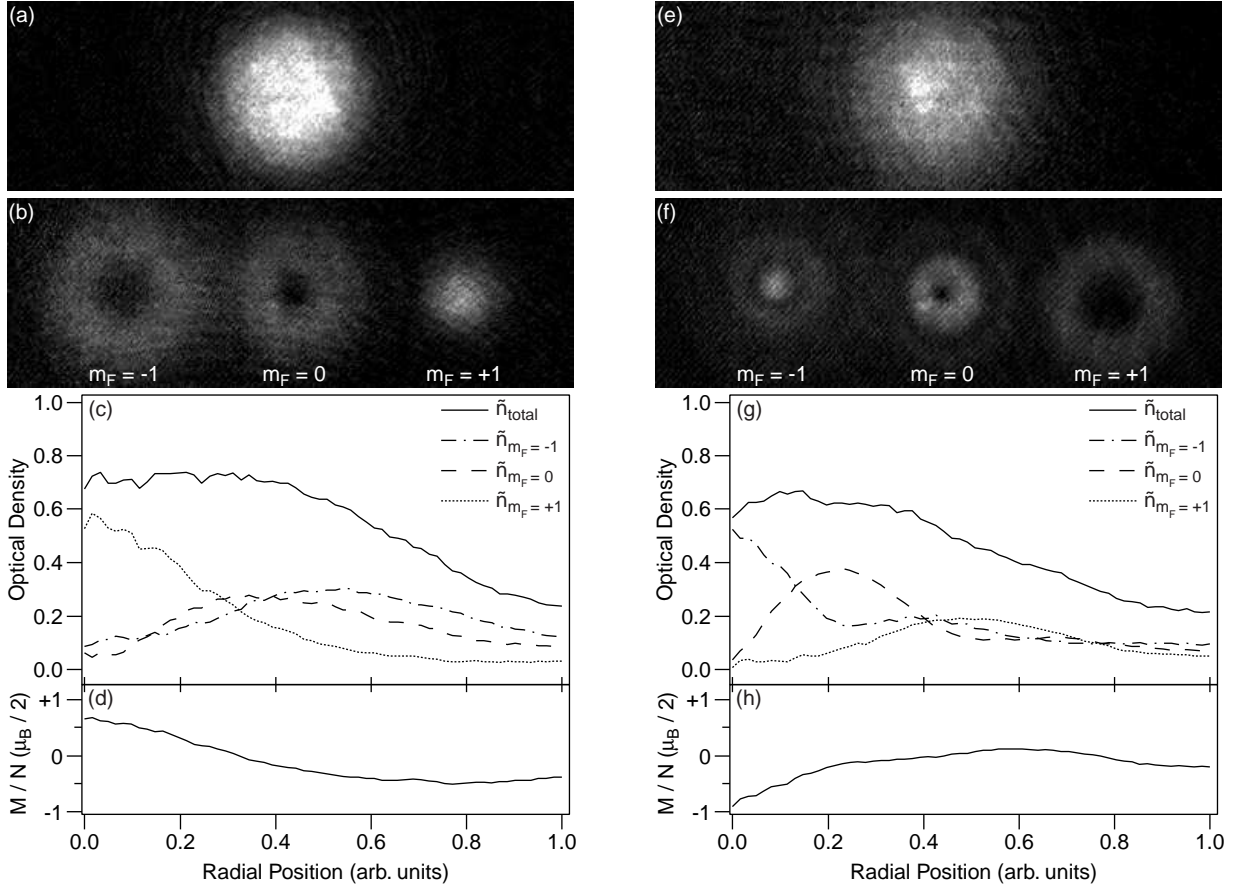


FIG. 2: Coreless vortex formation in a spinor Bose-Einstein condensate. Coreless vortices were imprinted by ramping $B_z \rightarrow 0$ and diagnosed by suddenly switching (a)-(d) $B_z \ll 0$ and (e)-(h) $B_z \gg 0$. Axial absorption images display the optical density of condensates after 20 ms of ballistic expansion (a,e) without and (b,f) with a magnetic field gradient applied to separate the different spin states. (c) and (g) Azimuthally averaged optical density vs radial position for spin components shown in (b) and (f), respectively. The radial separation of the spin states resulted from their relative phase windings and is a clear signature of the skyrmion/meron wavefunction [Eq. (4)]. (d,h) Axial magnetization per particle, $M/N = (\mu_B/2) \times (\tilde{n}_{m_F=+1} - \tilde{n}_{m_F=-1})/\tilde{n}_{total}$, vs radial position. The absorption imaging light was resonant with the $F = 2 \rightarrow F' = 3$ transition. The atoms were optically pumped into the $F = 2$ hyperfine level with a pulse resonant with the $F = 1 \rightarrow F' = 2$ transition. This provided equal imaging sensitivity to each spin state. The field of view in (a), (b), (e), and (f) is $1.0 \text{ mm} \times 3.0 \text{ mm}$.

the $\hat{n}(\phi)$ axis through an angle $\beta(r)$ [18]

$$|\zeta(r, \phi, z)\rangle = e^{-i(\vec{\mathcal{F}}/\hbar) \cdot \hat{n}(\phi)\beta(r)} |\zeta_0\rangle, \quad (3)$$

where $\vec{\mathcal{F}}$ is the spin operator and $|\zeta_0\rangle = |F, m_z = m_F\rangle$ is a polarized spinor. For $|\zeta_0\rangle = |1, -1\rangle$, Eq. (3) gives the condensate spinor in the laboratory frame as

$$|\zeta(r, \phi, z)\rangle = \frac{\cos^2(\beta(r)/2)}{\sqrt{2}} |1, -1\rangle + \frac{\sin(\beta(r))}{\sqrt{2}} e^{i\phi} |1, 0\rangle + \frac{\sin^2(\beta(r)/2)}{\sqrt{2}} e^{i2\phi} |1, +1\rangle. \quad (4)$$

$\beta(0) = 0$ and skyrmions (merons) are described by the boundary condition $\beta(\infty) = \pi$ ($\beta(\infty) = \pi/2$).

The radial dependence of $\beta(r)$ is determined by requir-

ing the Gross-Pitaevskii energy functional,

$$E = \int d^3\vec{r} n \left(\frac{\hbar^2}{2m} \langle \nabla \zeta | \nabla \zeta \rangle + V + \left(\frac{c_0}{2} + \frac{c_2}{2} \frac{|\vec{F}|^2}{\hbar^2} \right) n \right), \quad (5)$$

be stationary with respect to variations in β . In writing Eq. (5) we have made the Thomas-Fermi approximation, $\langle \nabla \zeta | \nabla \zeta \rangle = \sum_{m_z=-F}^F \nabla \zeta_{m_z}^\dagger \cdot \nabla \zeta_{m_z}$, $V = -g_F \mu_B \vec{F} \cdot \vec{B}/\hbar$, $\vec{F} = \langle \zeta | \vec{\mathcal{F}} | \zeta \rangle$, $c_0 = 4\pi\hbar^2 \bar{a}/m$, and $c_2 = 4\pi\hbar^2 \Delta a/m$. Here $\bar{a} = (2a_0 + a_2)/3$ and $\Delta a = (a_2 - a_0)/3$ characterize two-body interactions, where a_0 and a_2 are scattering lengths for collisions with total angular momentum $F = 0$ and $F = 2$, respectively [6]. For $a_2 > 0$ the atomic interactions are anti-ferromagnetic (polar), as in ^{23}Na [31], while for $a_2 < 0$ they are ferromagnetic, as in ^{87}Rb [32].

Using Eq. (4) as a trial spinor, we find that $\beta(r)$ satisfies the meron boundary conditions and varies from

$\beta(0) = 0$, due to the kinetic energy of the spin texture, to $\beta(\infty) = \pi/2$, due to the atomic Zeeman energy, over a characteristic length scale given by the larger of $(\hbar^2/mg_F\mu_B B')^{1/3}$ and $|B_z|/B'$, in reasonable agreement with the results presented in Fig. 2. We observed that the boundary condition $\beta(0) = 0$ was maintained regardless of the sign of B_z , i.e. atomic spins along the trap axis always remained in the initial state. This emphasizes the non-trivial topology of the spin texture. If the atomic spins had simply followed the local magnetic field, $\beta(r)$ would satisfy $\tan\beta(r) = B'r/B_z$. Thus, scanning B_z from slightly positive to slightly negative would instantaneously change the boundary condition at the origin from $\beta(0) = 0$ to $\beta(0) = \pi$ and flip the atomic spins along the trap axis.

The trial spinor in Eq. (4) does not have the most general form since it was derived by rotating a polarized spinor [Eq. (3)] and is inherently ferromagnetic, $|\vec{F}| = \hbar$. Accordingly, the spin-dependent interaction term in Eq. (5) does not vary with β and therefore does not contribute to the determination of $\beta(r)$. This restriction is not severe since the Zeeman energy dominates the spin-dependent interaction energy in our experiment.

It should be possible to overlap the condensate with an optical dipole trap so that, after ramping $B_z \rightarrow 0$, relaxing the radial magnetic field gradient would allow for the spin-dependent interactions to determine the evolution of the condensate. It is predicted that skyrmions/merons in condensates with anti-ferromagnetic (ferromagnetic) interactions are unstable (stable) [9, 10, 33, 34, 35, 36, 37, 38]. At present, excitations created during the field ramping process have prevented us from characterizing the stability of coreless vortices in an anti-ferromagnetic ^{23}Na condensate. However, we were able to imprint the spin texture in the presence of the optical dipole trap, as well as reproduce the results of Ref. [18] by fully inverting the axial bias field to produce vortices with a 4π phase winding in an optical dipole trap. At zero magnetic field, it may then be possible to observe multiply charged vortices in a spinor condensate “unwind” themselves as predicted in Ref. [6]. The unwinding process is precisely the position-dependent spin rotation demonstrated in previous work [18], with the spin texture investigated here as an intermediate state [37].

In conclusion, we have demonstrated a robust technique for creating coreless vortices in a Bose-Einstein condensate. Our technique can be extended to generate spin textures with arbitrary winding number and variable angular momentum per particle by using higher-order, axisymmetric multipole magnetic fields and condensates with different spin. This work opens up the opportunity to study the stability of topological defects in spinor Bose-Einstein condensates.

We are grateful to K. Machida for bringing the spin texture studied here to our attention. We thank T. Pasquini for experimental assistance and J.R. Anglin

and M. Crescimanno for valuable discussions. This work was funded by ONR, NSF, ARO, NASA, and the David and Lucile Packard Foundation.

* URL: http://cua.mit.edu/ketterle_group/

- [1] T. H. R. Skyrme, Proc. R. Soc. London A **260**, 127 (1961).
- [2] N. D. Mermin and T.-L. Ho, Phys. Rev. Lett. **36**, 594 (1976).
- [3] P. W. Anderson and G. Toulouse, Phys. Rev. Lett. **38**, 508 (1977).
- [4] R. Blaauwgeers, V. B. Eltsov, M. Krusius, J. J. Ruohio, R. Schanen, and G. E. Volovik, Nature **404**, 471 (2000).
- [5] D.-H. Lee and C. L. Kane, Phys. Rev. Lett. **64**, 1313 (1990).
- [6] T.-L. Ho, Phys. Rev. Lett. **81**, 742 (1998).
- [7] T. Ohmi and K. Machida, J. Phys. Soc. Jpn **67**, 1822 (1998).
- [8] S.-K. Yip, Phys. Rev. Lett. **83**, 4677 (1999).
- [9] U. A. Khawaja and H. Stoof, Nature **411**, 918 (2001).
- [10] U. A. Khawaja and H. T. C. Stoof, Phys. Rev. A **64**, 043612 (2001).
- [11] E. J. Yarmchuk, M. J. V. Gordon, and R. E. Packard, Phys. Rev. Lett. **43**, 214 (1979).
- [12] K. W. Madison, F. Chevy, W. Wohlleben, and J. Dalibard, Phys. Rev. Lett. **84**, 806 (2000).
- [13] J. R. Abo-Shaeer, C. Raman, J. M. Vogels, and W. Ketterle, Science **292**, 476 (2001).
- [14] M. R. Matthews, B. P. Anderson, P. C. Haljan, D. S. Hall, C. E. Wieman, and E. A. Cornell, Phys. Rev. Lett. **83**, 2498 (1999).
- [15] Y. V. Gott, M. S. Ioffe, and V. G. Tel'kovskii, Nuclear Fusion Supplement **3**, 1045 (1962).
- [16] D. E. Pritchard, Phys. Rev. Lett. **51**, 1336 (1983).
- [17] T. Isoshima, M. Nakahara, T. Ohmi, and K. Machida, Phys. Rev. A **61**, 063610 (2000).
- [18] A. E. Leanhardt, A. Görlitz, A. P. Chikkatur, D. Kielpinski, Y. Shin, D. E. Pritchard, and W. Ketterle, Phys. Rev. Lett. **89**, 190403 (2002).
- [19] M. V. Berry, Proc. R. Soc. Lond. A **392**, 45 (1984).
- [20] N. D. Mermin, Rev. Mod. Phys. **51**, 591 (1979).
- [21] T. L. Gustavson, A. P. Chikkatur, A. E. Leanhardt, A. Görlitz, S. Gupta, D. E. Pritchard, and W. Ketterle, Phys. Rev. Lett. **88**, 020401 (2002).
- [22] A. E. Leanhardt, A. P. Chikkatur, D. Kielpinski, Y. Shin, T. L. Gustavson, W. Ketterle, and D. E. Pritchard, Phys. Rev. Lett. **89**, 040401 (2002).
- [23] A. E. Leanhardt, Y. Shin, A. P. Chikkatur, D. Kielpinski, W. Ketterle, and D. E. Pritchard, cond-mat/0211345 (2002).
- [24] E. Lundh, C. J. Pethick, and H. Smith, Phys. Rev. A **58**, 4816 (1998).
- [25] F. Dalfovo and M. Modugno, Phys. Rev. A **61**, 023605 (2000).
- [26] J. Williams and M. J. Holland, Nature **401**, 568 (1999).
- [27] J. Ruostekoski, Phys. Rev. A **61**, 041603(R) (2000).
- [28] K.-P. Marzlin, W. Zhang, and B. C. Sanders, Phys. Rev. A **62**, 013602 (2000).
- [29] U. Leonhardt and G. E. Volovik, JETP Lett. **72**, 46 (2000).

- [30] J. Ruostekoski and J. R. Anglin, Phys. Rev. Lett. **86**, 3934 (2001).
- [31] J. Stenger, S. Inouye, D. M. Stamper-Kurn, H.-J. Miesner, A. P. Chikkatur, and W. Ketterle, Nature **396**, 345 (1998).
- [32] N. N. Klausen, J. L. Bohn, and C. H. Greene, Phys. Rev. A **64**, 053602 (2001).
- [33] R. A. Battye, N. R. Cooper, and P. M. Sutcliffe, Phys. Rev. Lett. **88**, 080401 (2002).
- [34] T. Mizushima, K. Machida, and T. Kita, Phys. Rev. Lett. **89**, 030401 (2002).
- [35] T. Isoshima and K. Machida, Phys. Rev. A **66**, 023602 (2002).
- [36] Y. Zhang, W.-D. Li, L. Li, and H. J. W. Müller-Kirsten, Phys. Rev. A **66**, 043622 (2002).
- [37] J.-P. Martikainen, A. Collin, and K.-A. Suominen, Phys. Rev. A **66**, 053604 (2002).
- [38] T. Mizushima, K. Machida, and T. Kita, Phys. Rev. A **66**, 053610 (2002).